Supplementary Material: *Using a Resistor Network to Simulate Charge Transport in Organic Semiconductors through Injection Layers and Transport Layers*

Oliver Petkau, Ali Deniz Özdemir, Franz Symalla, Wolfgang Wenzel

Supplementary Note 1: Parameters

Parameters as used for all simulations and mentioned in the formulas of the main article:

- Temperature $T = 300\,\mathrm{K}$
- Dielectric constant $\epsilon_r = 4$
- Coupling constant $j_0 = 0.001\,\mathrm{eV}$
- Decay length $\delta_0 = 0.1\,\mathrm{nm}$

The full input files for the different Kinetic Monte Carlo (KMC) simulations are attached as separate files to this supplementary material.

Supplementary Note 2: Convergence of the full KMC simulation

To test the convergence of the reference KMC simulations, a common test is to inspect the trajectories of the charge carriers. For a converged KMC simulation one expects a linear cumulative charge displacement over time. The trajectories of the reference simulations are shown in Supplementary Figure 1, Supplementary Figure 2 and Supplementary Figure 3. All trajectories show linear behavior, indicating a converged simulation. As seen particularly clearly in the 15% frame of Supplementary Figure 3, there are different slopes present in the same frame as they belong to the calculations performed at different voltages. Thus, one can distinguish four packs of trajectories corresponding to four of the voltages in this experiment.

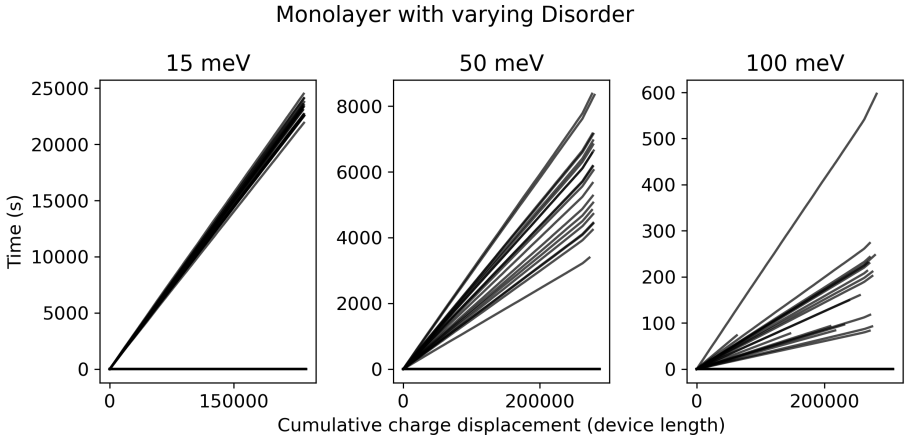

Supplementary Figure 1: **Monolayer Convergence** Inspection of the cumulative charge displacement in the Kinetic Monte Carlo simulations used as a reference. Shown are the calculations with varying energetic disorder. Different voltages are not distinguished. The displacement is in multiples of the device length.

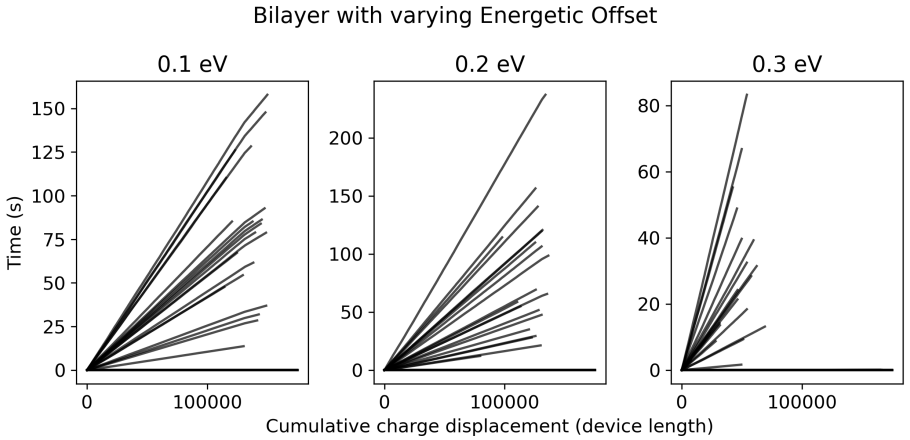

Supplementary Figure 2: **Bilayer Convergence** Inspection of the cumulative charge displacement in the Kinetic Monte Carlo simulations used as a reference. Shown are the calculations with varying energetic offsets. Different voltages are not distinguished. The displacement is in multiples of the device length.

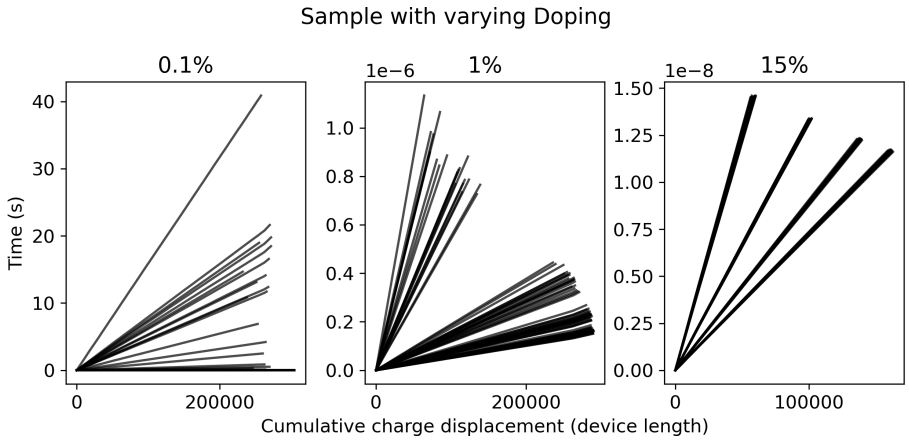

Supplementary Figure 3: **Doped System Convergence** Inspection of the cumulative charge displacement in the Kinetic Monte Carlo simulations used as a reference. Shown are the calculations with varying doping concentrations. Different voltages are not distinguished. The displacement is in multiples of the device length.

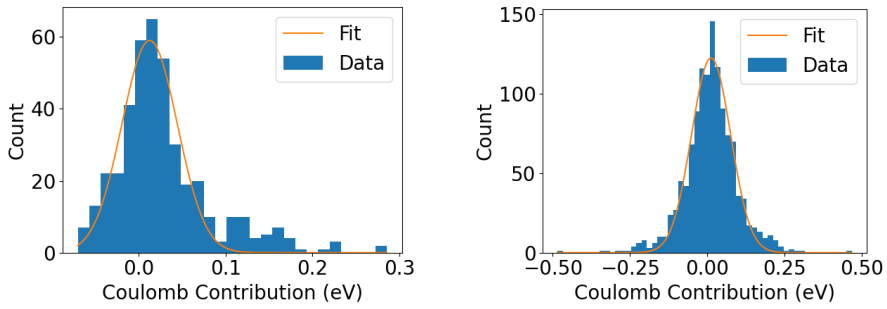

(a) Step 50

(b) Step 10^7

Supplementary Figure 4: **Fit of Coulomb Contributions** Gaussian distributions as fitted to the histograms of the Coulomb contribution at step 50 and step 10^7.

Supplementary Note 3: Coulomb Term and Occupation Probability

As discussed in the main paper the Coulomb interaction is a dynamic contribution to the energy difference as used to construct the resistors in the resistor model. These interaction terms are calculated starting from one node in the model and have to be calculated for all connections to this node. This can then be done for all nodes. In general, this interaction depends on the surrounding of this initial site, more precisely on the charge density surrounding the site. As charges will move through the sample over time, this charge density changes over time, making this quantity time dependent. This is not compatible with the time-averaged construction of the network. One idea to overcome this time dependency was to assume that the system will reach a steady state. In this case the Coulomb interaction terms calculated at any point after reaching the steady state will follow a distribution that is constant with time. It was further assumed that the charges are distributed sufficiently evenly so the Coulomb contribution could be drawn from this distribution.

To investigate this, Lightforge simulations were used to inspect the Coulomb interaction term at various time-steps throughout the simulation. To validate that the material was sufficiently evenly sampled the positions of the charge carriers were visually inspected using k-means clustering[5]. These interactions were put into a histogram and a Gaussian distribution was fitted to this histogram as depicted in Supplementary Figure 4 for two different snapshots during the simulation. The evolution of such fits during the KMC is depicted in Supplementary Figure 5. As shown there, the curves converge rapidly towards the final distribution, even though there are fluctuations even for time steps late into the simulation run. To further investigate the convergence behavior, the evolution

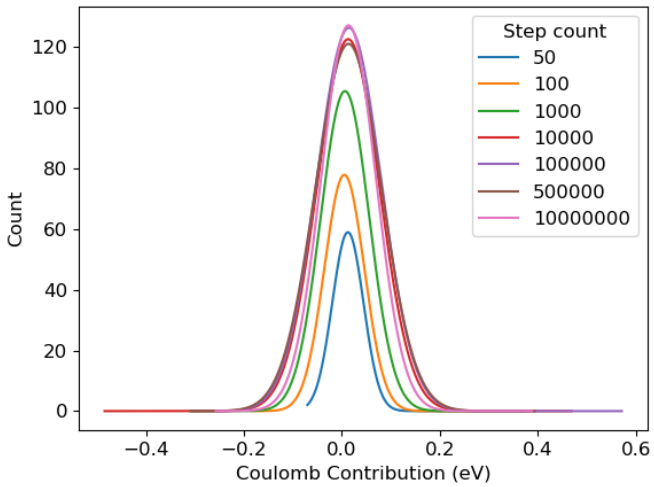

Supplementary Figure 5: **Convergence of Coulomb Interactions** Distribution of Coulomb interaction terms fitted to Lightforge outputs at different step counts during the simulation.

of the individual parameters is shown in the logarithmic plots in Supplementary Figure 6. All three parameters converge rather fast towards the final value, besides some remaining fluctuations. These findings suggest that the steady state is reached after only 10^5 simulation steps. Thus, this point was further used for all dynamic quantities taken out of KMC simulations and used to build the resistor models. This is in line with other literature suggesting, that a KMC simulation has to run for 10% of the overall runtime to become independent from the starting configuration[7].

Coulomb Term

With distributions in the form of Supplementary Figure 5 at hand the Coulomb interaction contribution could be drawn from the distribution for each constructed resistor. However, the results show only very poor agreement with the reference simulation, calculated by Lightforge. The simulation uses a system in the form of Supplementary Figure 7. To ensure high charge carrier concentrations, the sample is doped with a high concentration of dopants of 15 %. The size of the investigated material was $20\,\mathrm{nm} \times 20\,\mathrm{nm} \times 20\,\mathrm{nm}$. The energy distributions of both, host material and dopant material follow a Gaussian distribution with a disorder of $\sigma = 100\,\mathrm{meV}$. The mean values of the levels are shown in Supplementary Figure 7. As for all simulations, Lightforge was used to calculate 20 replicas of systems with the same distributions of energies, starting from different random seeds. At 10^5 steps the parameters for the 20 Resistor

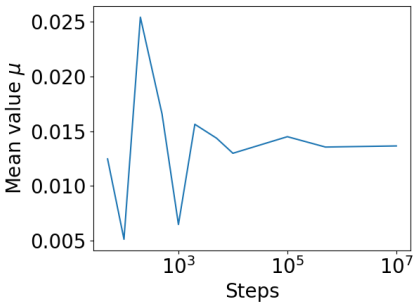

(a) Fit of the mean value μ

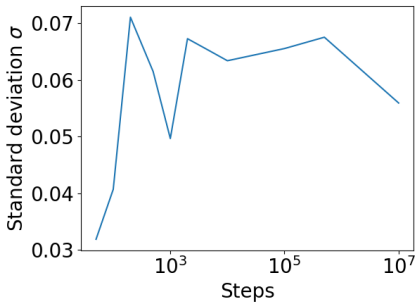

(b) Fit of the standard deviation σ

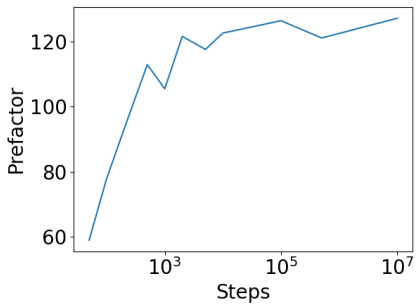

(c) Fit of the prefactor

Supplementary Figure 6: **Convergence of Fit Parameters** Evolution of the individual fit parameters of the Gaussian distribution to the histogram data for the energetic contributions by the Coulomb interaction.

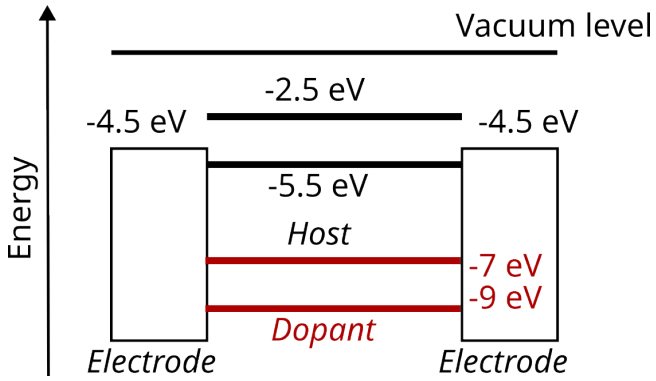

Supplementary Figure 7: **Test System for Coulomb Contribution Discussion** Energy diagram of the material used for the test regarding the simulation with explicit Coulomb contribution.

Network calculations are extracted. The reference values are the results taken from a full Lightforge simulation after $1.2 \cdot 10^6$ steps.

A comparison between the Lightforge simulation, the Resistor Network calculation using the Coulomb contribution as drawn from the obtained distribution and a Resistor Network calculation using the final implementation without the Coulomb contribution can be seen in Supplementary Figure 8. As seen in this figure, the random Coulomb contribution leads to very high uncertainties. The results are oftentimes multiple orders of magnitude apart from the reference values. Further, the uncertainties are always at least one order of magnitude larger than the calculated values. Such results are not only very unreliable, but also unusable. Thus, in an attempt to stabilize the contribution and in the hope of more reasonable uncertainties another calculation run was performed using only the mean value of the distribution as a contribution to the energy difference. The results of this calculation are shown in Supplementary Figure 9. As seen in this figure the Coulomb contribution still leads to a high uncertainty. Especially for low fields the uncertainty is one order of magnitude larger than the calculated value. For higher fields the uncertainty decreases. These results seem better than the results obtained before, but the results still deviate more from the reference value than the implementation without the Coulomb contribution.

Since agreement with the reference simulation is better without the Coulomb interactions contribution, the term was dropped entirely in the final implementation. The found steady state, however, was used to get the occupation probabilities for the individual sites.

While this explicit Coulomb contribution is dropped, the Coulomb interaction and especially the prohibition of double occupation of sites is treated implicitly by the use of the occupation probabilities in the resistor definition. Even

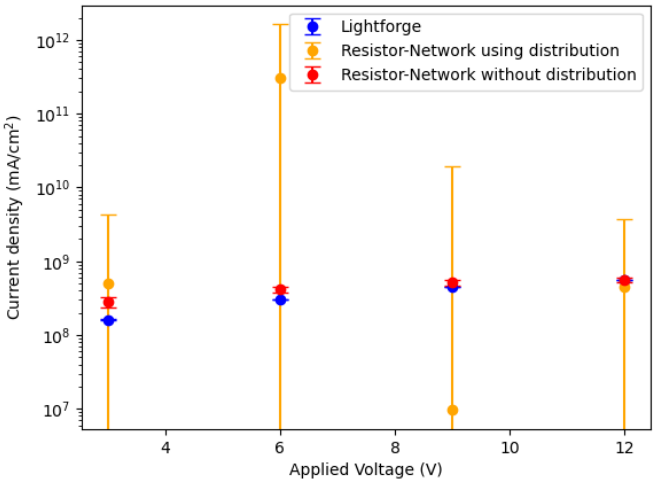

Supplementary Figure 8: **Considering the Coulomb Interaction by drawing from the fitted Distribution** A comparison of the simulation using the Resistor Network calculation with and without the Coulomb contribution. This contribution is drawn from a distribution of Coulomb interactions. Also, a full Kinetic Monte Carlo simulation is performed using Lightforge and the results are plotted for reference. Error bars correspond to the standard deviation to the mean value, obtained from multiple replica systems.

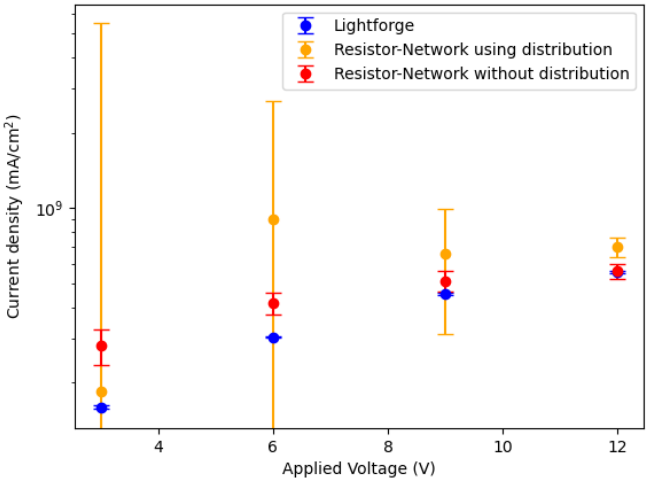

Supplementary Figure 9: **Considering the Coulomb Interaction by using the Mean of the fitted Distribution** A comparison of the simulation using the Resistor Network calculation with and without the Coulomb contribution. This contribution is this time taken as the mean value of the distribution of Coulomb interactions. Also, a full Kinetic Monte Carlo simulation is performed using Lightforge and the results are plotted for reference. Error bars correspond to the standard deviation to the mean value, obtained from multiple replica systems.

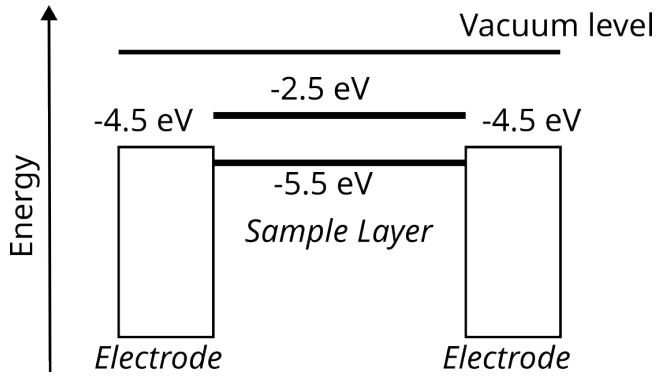

Supplementary Figure 10: **Test System for the Occupation Probability Discussion** Energy diagram of the monolayer material used for the simulation using the Fermi distribution to calculate the occupation probabilities.

though this would not explain the high uncertainty, considering the Coulomb interaction in the occupation probabilities and in the energy terms could lead to double counting.

Occupation Probability

The literature regarding percolation approaches suggests that the occupation probability for each site can be calculated using Fermi-Dirac statistics and estimating the Fermi-level by the mean between the highest occupied and the lowest unoccupied state, i.e. the middle of the band gap [1, 3]. This was tested and the results show poor agreement with the reference simulation. A comparison of the results with the reference simulation is depicted in Supplementary Figure 11. The tested system consists of a single layer as depicted in Supplementary Figure 10 with a disorder of 50 meV applied to the energy levels. Such a simple system was used to evade additional effects, like shifts of the Fermi level due to doping.

Using the Fermi distribution, results not only don't agree with the reference but are also unable to reproduce the general trend of higher current with higher applied fields. Thus, the occupation probabilities have to be obtained by other means. They can not be calculated analytically in closed form.

Köhler and Bässler state that the occupation probabilities in a high carrier regime can be taken as time-independent after some relaxation of the system [2, p. 223]. This would correspond to a steady state. With the steady state found previously by KMC simulation after 10^5 simulation steps, the occupation probabilities can therefore be read out from the KMC simulation after the relaxation. In the current state, the initial KMC simulation to determine the particle distributions cannot be avoided.

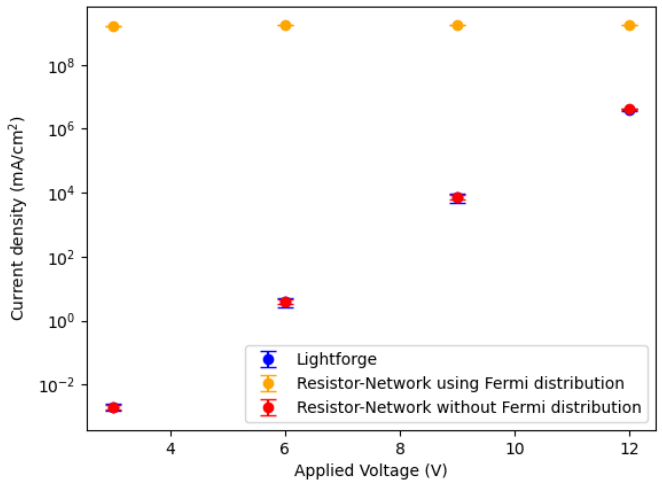

Supplementary Figure 11: **Results after using the Fermi Distribution** Comparison of the implementation using either the Fermi distribution or numerically obtained occupation probabilities. Also, a full Kinetic Monte Carlo simulation is performed using Lightforge and the results are plotted for reference. Error bars correspond to the standard deviation to the mean value, obtained from multiple replica systems.

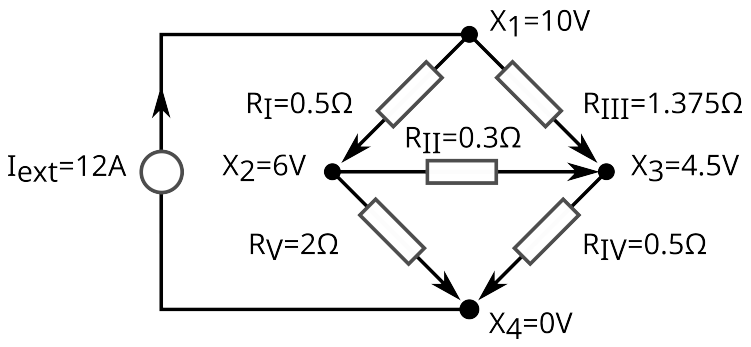

Supplementary Figure 12: **Wheatstone Bridge** Circuit diagram of a Wheatstone bridge with set potentials and resistances.

The second group of Resistor Network measurements in Supplementary Figure 11 are obtained by using occupation probabilities numerically calculated by Lightforge after 10^5 steps. There, the general trend as well as the values are in good agreement with the reference simulation. This implementation was used for all results in the main paper.

Supplementary Note 4: Wheatstone Bridge as an Example

A simple circuit is characterized and the currents within the system are calculated to illustrate the matrix method described in the main paper, following Strang[6, p. 110ff]. The chosen circuit is in a Wheatstone bridge geometry with set node potentials and resistances as depicted in Supplementary Figure 12. A similar setup can be found in an article by Mishra and Barman[4].

Following Strang, the vector of currents $\vec{I}$ in a system with an external current source $\vec{F}$ is given as[6, p. 110ff]

$$\vec{I} = -\hat{C} \cdot \hat{A} \cdot \vec{X} \tag{1}$$

with the conduction matrix $\hat{C}$, the adjacency matrix $\hat{A}$ and the vector of nodal potentials $\vec{X}$. The first step will be the construction of the adjacency matrix $\hat{A}$. The system has four nodes labeled with Arabic numerals and five edges labeled with Roman numerals. Hence, the adjacency matrix is of shape 5×4. It is useful to visualize the direction of measured currents by arrows along the edges before determining the entries in the matrix. Here the convention is used that a current is measured as positive if the current is flowing from a node with lower number to a node with a higher nodal number.

Supplementary Table 1: Construction of the entries in the adjacency matrix for the Wheatstone bridge with the node numbers and edge numbers.

	1	**2**	**3**	**4**
I				
II				
III	1	0	-1	0
IV				
V				

Supplementary Table 2: Entries for the full adjacency matrix for the Wheatstone bridge with the node numbers and edge numbers.

	1	**2**	**3**	**4**
I	1	-1	0	0
II	0	1	-1	0
III	1	0	-1	0
IV	0	0	1	-1
V	0	1	0	-1

For the entries it is easiest to construct either columnwise, looking at one node at a time and noting down all connected edges with the corresponding signs or rowwise, looking at an edge and noting start point and end point in the matrix. The rowwise approach for edge III is depicted in Supplementary Table 1. There the edge III is connecting node 1 and 3 hence the corresponding values are non-zero. The direction of measured current is set from lower to higher node number, Hence, it is outgoing of node 1, depicted by the positive sign and incoming to node 3 depicted by a negative sign. In this manner the table can be filled resulting in Supplementary Table 2 or rewritten as the resulting matrix

$$\hat{A} = \begin{pmatrix} 1 & -1 & 0 & 0 \\ 0 & 1 & -1 & 0 \\ 1 & 0 & -1 & 0 \\ 0 & 0 & 1 & -1 \\ 0 & 1 & 0 & -1 \end{pmatrix} \tag{2}$$

Next up, one can directly collect the resistances and node potentials from Supplementary Figure 12:

$$\hat{R} = \begin{pmatrix} R_I & 0 & 0 & 0 & 0 \\ 0 & R_{II} & 0 & 0 & 0 \\ 0 & 0 & R_{III} & 0 & 0 \\ 0 & 0 & 0 & R_{IV} & 0 \\ 0 & 0 & 0 & 0 & R_V \end{pmatrix} = \begin{pmatrix} 0.5 & 0 & 0 & 0 & 0 \\ 0 & 0.3 & 0 & 0 & 0 \\ 0 & 0 & 1.375 & 0 & 0 \\ 0 & 0 & 0 & 0.5 & 0 \\ 0 & 0 & 0 & 0 & 2 \end{pmatrix} \Omega \tag{3}$$

$$\vec{X} = \begin{pmatrix} X_1 \\ X_2 \\ X_3 \\ X_4 \end{pmatrix} = \begin{pmatrix} 10 \\ 6 \\ 4 \\ 0 \end{pmatrix} \text{ V} \tag{4}$$

Also, the unknown vector of edge currents can be established as

$$\vec{I} = \begin{pmatrix} I_I \\ I_{II} \\ I_{III} \\ I_{IV} \\ I_V \end{pmatrix} \tag{5}$$

The circuit does not contain additional potential sources, but an additional current source so that

$$\vec{F} = \begin{pmatrix} -12 \\ 0 \\ 0 \\ 12 \end{pmatrix} \text{ A} \tag{6}$$

After inverting the resistance matrix in Supplementary Equation 3

$$\hat{C} = \begin{pmatrix} \frac{1}{R_I} & 0 & 0 & 0 & 0 \\ 0 & \frac{1}{R_{II}} & 0 & 0 & 0 \\ 0 & 0 & \frac{1}{R_{III}} & 0 & 0 \\ 0 & 0 & 0 & \frac{1}{R_{IV}} & 0 \\ 0 & 0 & 0 & 0 & \frac{1}{R_V} \end{pmatrix} = \begin{pmatrix} \frac{1}{0.5} & 0 & 0 & 0 & 0 \\ 0 & \frac{1}{0.3} & 0 & 0 & 0 \\ 0 & 0 & \frac{1}{1.375} & 0 & 0 \\ 0 & 0 & 0 & \frac{1}{0.5} & 0 \\ 0 & 0 & 0 & 0 & \frac{1}{2} \end{pmatrix} \Omega^{-1} \tag{7}$$

and since there are no external potential sources in the system, Supplementary Equation 1 can be used to calculate the edge currents as

$$\vec{I} = -\hat{C} \cdot \hat{A} \cdot \vec{X} = \begin{pmatrix} -\frac{4}{0.5} \\ -\frac{1.5}{0.3} \\ -\frac{5.5}{1.375} \\ -\frac{4.5}{0.5} \\ -\frac{6}{2} \end{pmatrix} \text{ A} = \begin{pmatrix} -8 \\ -5 \\ -4 \\ -9 \\ -3 \end{pmatrix} \text{ A} = \begin{pmatrix} I_I \\ I_{II} \\ I_{III} \\ I_{IV} \\ I_V \end{pmatrix} \tag{8}$$

In this way the currents for all unknown connections can be calculated systematically with the knowledge of the nodal potentials and the resistances.

Supplementary References

[1] Andreas Hofacker. "Critical charge transport networks in doped organic semiconductors". en. In: *Communications Materials* 1.1 (Nov. 2020). Number: 1, pp. 1–9. ISSN: 2662-4443. DOI: 10.1038/s43246-020-00091-1. URL: https://www.nature.com/articles/s43246-020-00091-1 (visited on 06/11/2023).

[2] Anna Köhler and Heinz Bässler. *Electronic Processes in Organic Semiconductors: An Introduction*. en. 1st ed. Wiley, May 2015. ISBN: 978-3-527-33292-2 978-3-527-68517-2. DOI: 10.1002/9783527685172. URL: https://onlinelibrary.wiley.com/doi/book/10.1002/9783527685172 (visited on 03/23/2024).

[3] Ling Li and Hans Kosina. "Charge Transport in Organic Semiconductor Devices". In: *Advances in Polymer Science*. Vol. 223. Journal Abbreviation: Advances in Polymer Science. Jan. 1970, pp. 301–323. ISBN: 978-3-642-04537-0. DOI: 10.1007/12_2009_14.

[4] Rajat Chandra Mishra and Himadri Barman. "Effective resistances of two-dimensional resistor networks". en. In: *European Journal of Physics* 42.1 (Nov. 2020), p. 015205. ISSN: 0143-0807. DOI: 10.1088/1361-6404/abc526. URL: https://dx.doi.org/10.1088/1361-6404/abc526 (visited on 06/09/2023).

[5] Dan Pelleg and Andrew Moore. "Accelerating exact k -means algorithms with geometric reasoning". en. In: *Proceedings of the fifth ACM SIGKDD international conference on Knowledge discovery and data mining*. San Diego California USA: ACM, Aug. 1999, pp. 277–281. ISBN: 978-1-58113-143-7. DOI: 10.1145/312129.312248. URL: https://dl.acm.org/doi/10.1145/312129.312248 (visited on 10/08/2024).

[6] Gilbert Strang. *Introduction to Applied Mathematics*. eng. Wellesley: Wellesley-Cambridge Press, 1986. ISBN: 978-0-9614088-0-0. URL: http://archive.org/details/introductiontoap0000stra (visited on 06/22/2023).

[7] Karin Zojer. "Simulation of Charge Carriers in Organic Electronic Devices: Methods with their Fundamentals and Applications". en. In: *Advanced Optical Materials* 9.14 (2021), p. 2100219. ISSN: 2195-1071. DOI: 10.1002/adom.202100219. URL: https://onlinelibrary.wiley.com/doi/abs/10.1002/adom.202100219 (visited on 06/07/2023).